



HAL
open science

Molecular Dynamics Simulation Study of Organic Solvents Confined in PIM-1 and P84 Polyimide Membranes

M.-L. Ouinten, Anthony Szymczyk, Aziz Ghoufi

► **To cite this version:**

M.-L. Ouinten, Anthony Szymczyk, Aziz Ghoufi. Molecular Dynamics Simulation Study of Organic Solvents Confined in PIM-1 and P84 Polyimide Membranes. *Journal of Physical Chemistry B*, 2023, 127 (5), pp.1237-1243. 10.1021/acs.jpccb.2c05796 . hal-03971812

HAL Id: hal-03971812

<https://hal.science/hal-03971812v1>

Submitted on 2 Mar 2023

HAL is a multi-disciplinary open access archive for the deposit and dissemination of scientific research documents, whether they are published or not. The documents may come from teaching and research institutions in France or abroad, or from public or private research centers.

L'archive ouverte pluridisciplinaire **HAL**, est destinée au dépôt et à la diffusion de documents scientifiques de niveau recherche, publiés ou non, émanant des établissements d'enseignement et de recherche français ou étrangers, des laboratoires publics ou privés.

Molecular Dynamics Simulation Study of Organic Solvents Confined in PIM-1 and P84 Polyimide Membranes

Mohammed-Lamine Quinten,^{†,‡} Anthony Szymczyk,^{*,‡} and Aziz Ghoufi^{*,†}

[†]*Univ Rennes, CNRS, IPR (Institut de Physique de Rennes) - UMR 6251, F-35000
Rennes, France*

[‡]*Univ Rennes, CNRS, ISCR (Institut des Sciences Chimiques de Rennes) - UMR 6226,
F-35000 Rennes, France*

E-mail: Anthony.szymczyk@univ-rennes1.fr; aziz.ghoufi@univ-rennes1.fr

Abstract

Organic solvent nanofiltration (OSN) has recently proved to be a promising separation process thanks to the development of membrane materials with suitable resistance towards organic solvents. Among those materials, P84 polyimide membranes are currently the most used in OSN while PIM-1 membranes have recently attracted attention due to their high permeance in apolar solvents and alcohols. Both P84 and PIM-1 membranes have nanosized free volumes and their separation performance is finely connected to polymer/solvent interactions. Consequently, modeling OSN membranes at the molecular scale is highly desirable in order to rationalize experimental observations and gain a deeper insight into the molecular mechanisms ruling solvent and solute permeation. A prerequisite for understanding solvent transport through OSN membranes is therefore to characterize the membrane/solvent interactions at the molecular level. For that purpose, we carried out molecular simulations of three different solvents, acetone, methanol and toluene in contact with P84 and PIM-1 membranes. The solvent uptake by both membranes was found to be correlated to the degree of confinement of the solvent, the polymer swelling ability and polymer/solvent interactions. The translational dynamics of the solvent molecules in the PIM-1 membrane was found to be correlated with the solvent viscosity due to the relatively large pores of this membrane. That was not the case with the P84 membrane, which has a much denser structure than the PIM-1 membrane, and for which it was observed that the translational dynamics of the confined solvent molecules was directly correlated to the affinity between the P84 polymer and the solvent.

Introduction

The past three decades membrane technologies have proved to be powerful sustainable processes.¹ Although they have been widely studied and used for water treatment (drinking water production, wastewater treatment, etc.), their use for the treatment of organic solvents has been much less studied, which is explained by the low resistance of traditional polymer membranes in organic solvents.² New polymer membranes with improved resistance towards organic solvents have been recently developed, making the emergence of the organic solvent nanofiltration (OSN) possible.³ Similar to the membrane processes used for water desalination, OSN is a pressure-driven process using membranes with nanometric pores or free volumes. It has already demonstrated great potential in petrochemical,⁴ pharmaceutical⁵ and catalytic⁶ applications due to high selectivity, low energy consumption and environmental footprint.

Among the different polymers that have been considered for OSN applications, P84 polyimide and polydimethylsiloxane (PDMS) membranes have been found to have a high chemical resistance in a variety of organic solvents such as acetone, toluene and hexane.⁷ More recently, the intrinsically microporous polymer PIM-1 has been shown to exhibit high permeance in apolar solvents and alcohols compared to commercial polyimide membranes.⁸ In both P84 and PIM-1 membranes, transport properties are controlled by phenomena occurring at the nanometer scale as the mean pore size of those membranes is around 10 Å or less. Modeling those OSN membranes at the molecular scale is then crucial to identify and rationalize the various phenomena ruling their separation performance. In this regard, molecular dynamics simulations appear as a powerful tool capable of shedding light on transport phenomena through OSN membranes.

However, molecular simulation has been little used for the study of OSN membranes so far. Jiang et al. have examined the structure of PIM-1 and polyimide (6FDA-ODA and polybenzimidazol) membrane upon solvent uptake⁹⁻¹¹ by using molecular simulation. Their membrane models have been validated by comparing the swelling degrees and pore size distributions with experiments. They have studied polymer/solvent interactions from binding energy calculations and have highlighted the connection between the solvent

permeability and the structural characteristics of the PIM-1 membrane.^{9,12} Moreover, they have investigated the influence of the chemical functionalization of PIM-1 on the solvent and solute permeability. More recently, interactions between the PIM-1 membrane and organic solvents such as toluene and methanol (pure solvents and mixtures) have been studied from atomistic simulations.¹³ The host-guest and guest-guest interactions have been investigated by means of radial distribution functions and specific interactions between the PIM-1 membrane and the hydroxyl group of methanol molecules as well as the aromatic rings of toluene molecules have been highlighted. P84 membranes have been even less studied from molecular simulations as, to our knowledge, only one work has been reported so far¹⁴ despite the fact that P84 is currently one of the most widely used polymer in OSN. In the present work, we used molecular dynamics simulations to investigate both the structure and the dynamics of three organic solvents with different physicochemical properties (acetone, toluene and methanol) confined in P84 and PIM-1 membranes and their specific interactions with these two membrane materials.

Methods

Membrane construction

The construction of the P84 and PIM-1 membranes was performed by means of the polymerization approach developed by Abbot et al. and implemented in the Polymatic code¹⁵ using LAMMPS¹⁶ as molecular dynamics (MD) package. It has been established that this methodology is suited for building amorphous polymers, such as PIM-1.^{15,17}

P84 is a mixture of two homopolymers with a ratio of repetitive units of 80:20 (see Figure 1a). As shown in Figure 1b, the PIM-1 repeat unit contains two rigid parts connected by a twisted spiro-carbon. For the PIM-1 membrane, 230 repeat units were randomly inserted into a simulation box of dimensions 40x40x150 Å. For the P84 membrane, 50 repetitive units A and 199 repetitive units B (see Figure 1a) were added in a box with the same dimensions as the PIM-1 membrane. The methodology proposed by Larsen et al.¹⁷ was followed in this work. The equilibration of the simulation box containing the repeat

units was performed in the NVT statistical ensemble (N, V and T are the number of particles, the volume and the temperature, respectively) at T=300 K, followed by an MD run in the NpT statistical ensemble (p is the pressure) at T = 300 K and p = 1 bar. In order to be consistent with experiments¹⁸ and to avoid too high-energy states, a capping of the final polymer configuration was performed by adding hydrogen atoms.¹⁷ For the PIM-1 membrane, the polymerization step led to polydisperse polymer chains ranging from 2 to 52 monomers. The polymer chains containing less than 10 monomers were removed, based on the work of Larsen et al.¹⁷ that showed they were not representative. Three independent polymerizations were carried out to ensure reproducibility and to reduce statistical errors. The PIM-1 membranes were then formed by 5 chains containing between 16 and 52 repeat units, which was close to the PIM-1 molecular model obtained by Larsen et al.¹⁷ For the P84 membrane, the three independent configurations were formed by (i) two polymer chains of 12 and 38 monomers A and six chains of 20, 20, 21, 22, 41 and 75 monomers B, (ii) three polymer chains of 15, 16 and 19 monomers A and six polymer chains of 23,25,25,31,36 and 56 monomers B, and (iii) two chains of 18 and 32 monomers A and five chains of 20,29,33,55 and 62 monomers B. The resulting OSN membranes were further equilibrated by following the protocol developed by Hofmann et al.,¹⁹ which is based on 7 cycles of 3 MD simulations each. The details for each step can be found elsewhere.^{13,20,21} Figures 1a and 1b show examples of final configurations for the P84 and PIM-1 membranes.

Molecular dynamics simulation procedure

The PIM-1 polymer was described by a united-atom model so that the CH_x (x = 1,2 or 3) groups were modeled as single particles. The energy of the system was described from the GAFF force field,²² which was found to reproduce well the structural properties of the PIM-1 polymer.^{20,23} The P84 polyimide membrane was modeled by means of the GAFF potential.²² Toluene (Tol), acetone (Ac) and methanol (MeOH) were described by the OPLS force field²⁴ that was found to reproduce well their thermodynamics properties.^{24,25}

The interactions between the membranes and the three solvents were considered as

a combination of electrostatic and van der Waals (VDW) interactions. In the GAFF and the OPLS force fields, VDW interactions are modeled 12-6 Lennard-Jones (LJs) potentials, respectively.

The electrostatic interactions were computed from the Ewald sum method.^{26,27} All interactions were truncated by using a cutoff of 12 Å. Simulations were performed using the LAMMPS MD package.¹⁶ The velocity Verlet propagator combined with the Nose-Hoover thermostat was considered.²⁸ A relaxation time of 0.5 ps was used. The acquisition phase was conducted over the last 20 ns of the simulation after a 50-ns equilibration stage and with a timestep of 1 fs. Periodic boundary conditions were applied in the three directions.

The solvent uptake was evaluated from the method developed by Ghoufi et al.²⁹ and consisting in explicit modeling of the polymer/solvent interface. As highlighted in Figure 1c, two reservoirs with 2000 molecules of solvent were added on each side of the membrane and MD simulations were carried out in the anisotropic Np_nT statistical ensemble, where p_n is the pressure along the normal to the polymer interface (i.e. the z-direction). An anisotropic Nose-Hoover barostat^{28,29} with a relaxation time of 0.5 ps was used.

Several properties such as the pore size distribution (PSD), the mean square displacement (MSD), the radial distribution function (RDF) and the number of hydrogen bonds per MeOH molecule (nHB) were evaluated. The PSD was calculated from the Zeo++ software³⁰ based on the Voronoi decomposition, which provides a graphical representation of the void space for a given arrangement of atoms in a periodic domain. The resulting Voronoi network was analyzed to obtain the diameter of the largest included sphere and the largest free sphere, which are two geometrical parameters that are frequently used to describe pore geometry. The mean pore diameter (MPD) was calculated as the average of the distribution. The MSD was calculated from the time correlation function $MSD(t) = \frac{\langle \sum_{t_0} \sum_{i=1}^N [\mathbf{r}_{com,i}(t+t_0) - \mathbf{r}_{com,i}(t_0)]^2 \rangle}{NN_0t}$ where $\mathbf{r}_{com,i}$ is the position of the center of mass of the molecule i , t_0 is the time origin, N is the number of molecules and N_0 is the number of t_0 . The nHB was determined by considering the geometrical criteria established by Chandler and Luzar,³¹ i.e. a hydrogen bond was formed if the distance between the

hydrogen and oxygen atoms of two molecules is smaller than 2.5 Å and if the distance between the oxygen atoms of these two molecules is smaller than 3.5 Å. By considering these two distance criteria, the angle criterion corresponding to an angle between the O–H and O–O vectors smaller than 30° was fulfilled. The RDF defines the probability of finding a particle at a distance r from another particle from the following relation, $RDF = dn_r / 4\pi r^2 dr \rho$, where dn_r is a function giving the number of particles within a shell of thickness dr and ρ is the density.

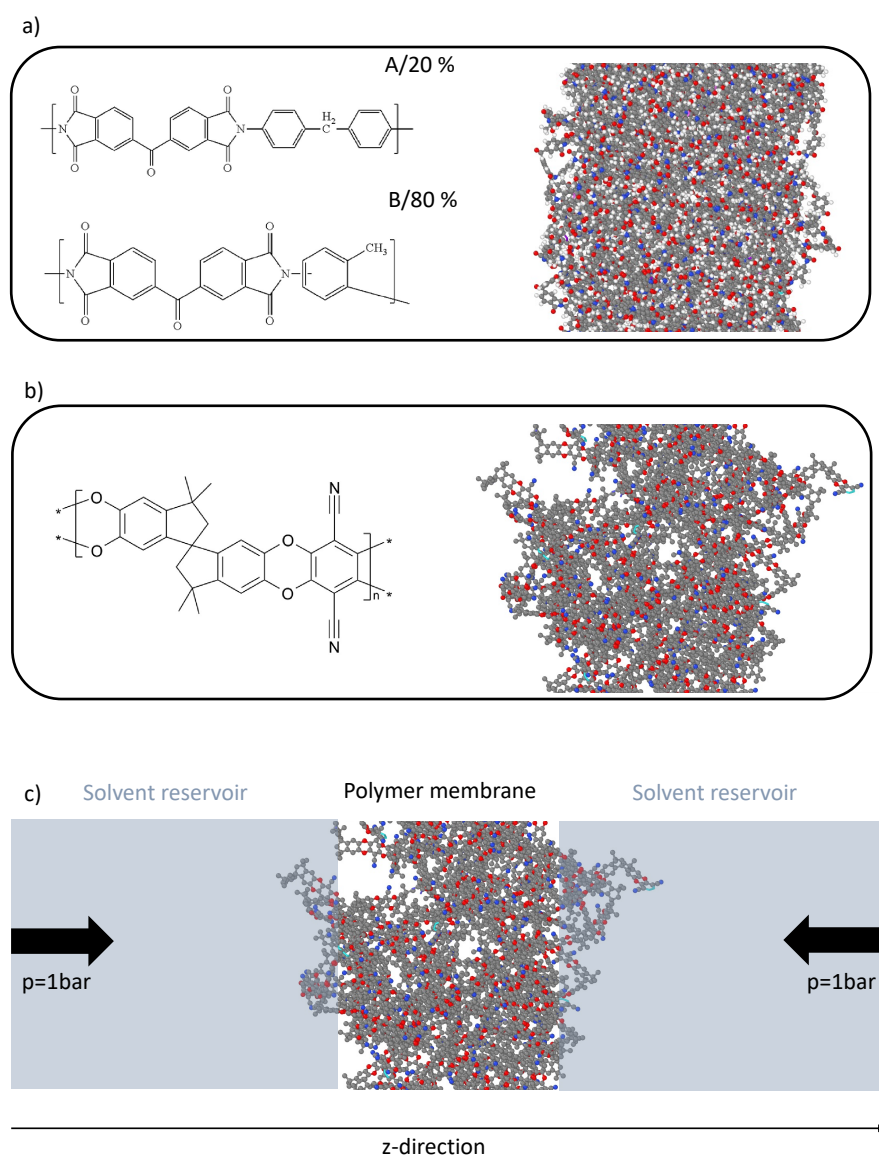


Figure 1: Repetitive units used to develop the molecular models of a) the P84 membrane and b) the PIM-1 membranes and examples of final configurations. c) Illustration of the method used to determine the solvent uptake in the $N_p n T$ statistical ensemble.

Results and Discussion

We report in Figures 2a and 2b the solvent uptake (%wt) by the P84 and PIM-1 membranes, determined from the ratio between the mass of solvent in the membrane and the polymer mass, as a function of time. As shown in Figure 2a, a limited solvent sorption by the P84 polyimide membrane was found, ranging from 8 %wt for Tol and Ac to 12 %wt for MeOH. The good reproducibility of the results is illustrated by the values of the MeOH uptake by the P84 membrane, namely 11.9 %wt, 12.1 %wt and 11.9 %wt, obtained from three independent configurations (see Membrane Construction section). Conversely, as highlighted in Figure 2b, the solvent uptake by the PIM-1 membrane was found much higher, ranging from 70-75 %wt for MeOH and Tol up to 102 %wt for Ac. It is worth mentioning that even for the highest mass uptake, the PIM-1 membrane did not dissolve into the solvent as shown by the value of the MPD and the PSD (Figures 2c and 2d). The different behaviors of the two membranes partly result from different steric constraints. Indeed, as shown in Figure 2c, the MPD of the PIM-1 and P84 membranes in the dry state was 7.4 Å and 6.2 Å respectively. However, Figure 2c shows a significant increase in the MPD of the solvated PIM-1 membrane, with an increase of 65 % (MPD=12 Å), 70 % (MPD=12.6 Å) and 55 % (MPD=11.2 Å) when brought into contact with MeOH, Ac and Tol, respectively. These results suggest a substantial swelling of the PIM-1 membrane in the three solvents unlike the P84 membrane for which no significant increase in the MPD was observed. The following swelling degrees (SD) of the P84 membrane were estimated from $SD=100(l_w-l_d)/l_d$, where l_w and l_d denote the membrane thickness in the wet and dry states, respectively (i.e. the membrane length according to the z direction (see Figure 1), which was evaluated from the atomic density profile) : $SD(\text{MeOH}) = 12\%$, $SD(\text{Ac}) = 4\%$ and $SD(\text{Tol}) = 9.4\%$.

The different behaviors of the PIM-1 and P84 membranes can be explained, at least partly, by the chemical structure of the two membranes. Indeed, as can be seen from Figure 1b, the repeat unit in PIM-1 has two rigid parts connected by a twisted spiro-carbon. It limits the entanglement of the polymer chains and explains the PIM-1 intrinsic microporosity as well as the substantial solvent uptake by this membrane. The chemical

structure of the P84 membrane (see Figure 1a) allows for a better entanglement of the polymer chains, which limits their degrees of freedom when the membrane is brought into contact with the solvent molecules.

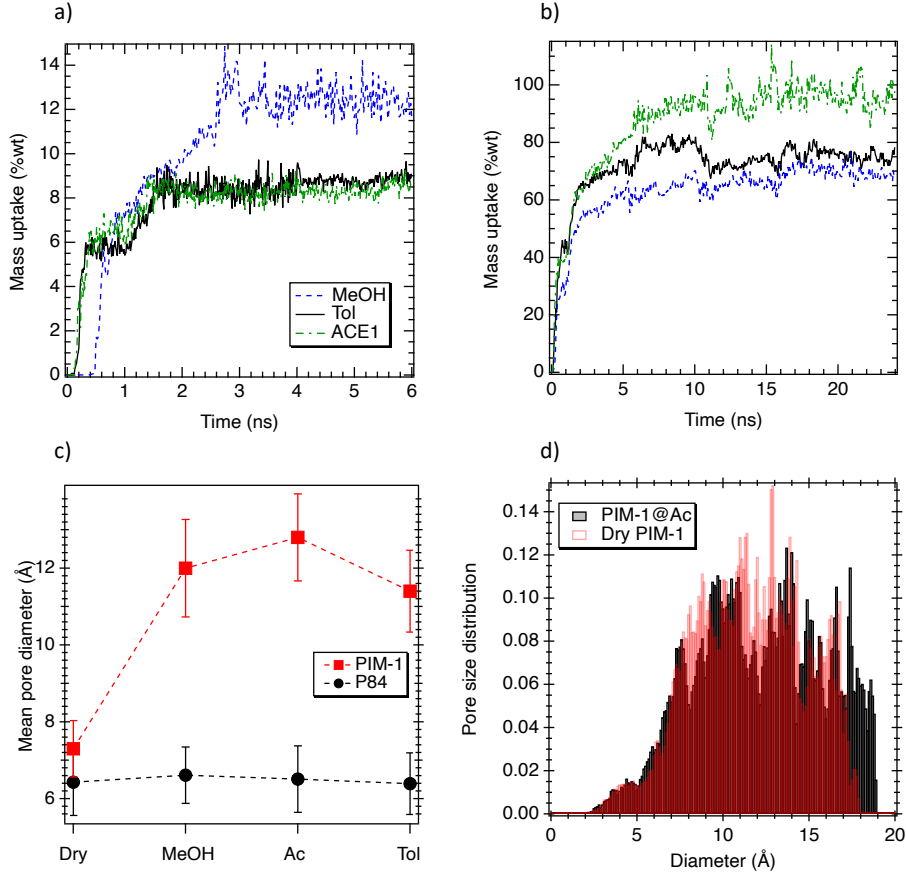


Figure 2: Mass uptake of toluene, acetone, and methanol as a function of time in a) the P84 membrane and b) the PIM-1 membrane. c) Mean pore diameter as a function of solvent in the P84 and PIM-1 membranes. d) Pore size distribution in the dry PIM-1 and PIM-1 solvated by Ac.

According to Figure 2a, the filling time (t_f), defined as the time needed to observe the temporal stabilization of the solvent uptake, follows the order $\text{MeOH} < \text{Ac} < \text{Tol}$ ($t_{f,\text{MeOH}} = 1.7 \text{ ns}$, $t_{f,\text{Ac}} = 3 \text{ ns}$ and $t_{f,\text{Tol}} = 4 \text{ ns}$) for the P84 membrane. This sequence can be partly correlated to the kinetic diameters of the solvent molecules as $d_{\text{MeOH}} = 3.8 \text{ \AA}$, $d_{\text{Ac}} = 4.7 \text{ \AA}$ and $d_{\text{Tol}} = 5.7 \text{ \AA}$. Unlike the P84 membrane, no correlation between the filling time and the kinetic diameter of the solvent molecules was observed with the PIM-1 membrane as t_f was found similar for the three solvents (see Figure 2b).

Figure 3a shows that the sequence of the solvent MSDs in the bulk phase was in

line with their viscosities (η_{Ac} (0.3 mPa s) $<$ η_{MeOH} (0.51 mPa s) \sim η_{Tol} (0.53 mPa s)). It is worth mentioning that only the solvent molecules that remained confined in the membrane were considered for MSD calculations. As expected, the MSD of the three solvents was found smaller in the PIM-1 membrane than in the bulk phase (by about one order of magnitude) but the sequence remained the same (see Figure 3b). Indeed, the MPD of the solvated PIM-1 membrane is relatively large (see Figure 2c), which limits confinement effects and thus leads to a bulk-like behavior (but with slower dynamics) for which solvent diffusion and viscosity are directly related by the Stokes-Einstein equation, i.e. $D = k_B T / (6\pi\eta R)$ where D is the diffusion coefficient, k_B is the Boltzmann constant, T is the temperature and R is the hydrodynamic radius. As can be seen in Figure 3c, no linear regime was observed for the organic solvents confined into the P84 membrane, which results from a higher confinement degree in the P84 matrix. Indeed, the MSDs of the three solvents were found to be about two orders of magnitude smaller in the P84 membrane than in the PIM-1 membrane. Moreover, unlike the PIM-1 membrane, no correlation was found between the MSDs of the solvents confined in the P84 membrane and their viscosities. It indicates that the solvents confined in the P84 membrane no longer behaves as bulk-like liquids, which results from the extreme confinement degree in the very dense P84 matrix. In this case, the MSDs are expected to be strongly impacted by the solvent / membrane specific interactions.

We report in Figure 4a the z-axis profile (i.e. along the normal to the membrane/reservoir interface; see Figure 1c) of the number of hydrogen bonds (per molecule), nHB , between the MeOH molecules themselves and between the MeOH molecules and the oxygen and nitrogen atoms of the P84 membrane. The number of hydrogen bonds between the MeOH molecules was found to decrease inside the membrane, by about one bond per molecule, which results from the high confinement degree within the P84 matrix. The loss of hydrogen bonds between the confined MeOH molecules was partly compensated by the formation of additional hydrogen bonds between MeOH molecules and interaction sites of the P84 membrane (up to 0.5 bond per MeOH molecule). Such favorable interactions contribute to the higher MeOH uptake by the P84 membrane compared to the other sol-

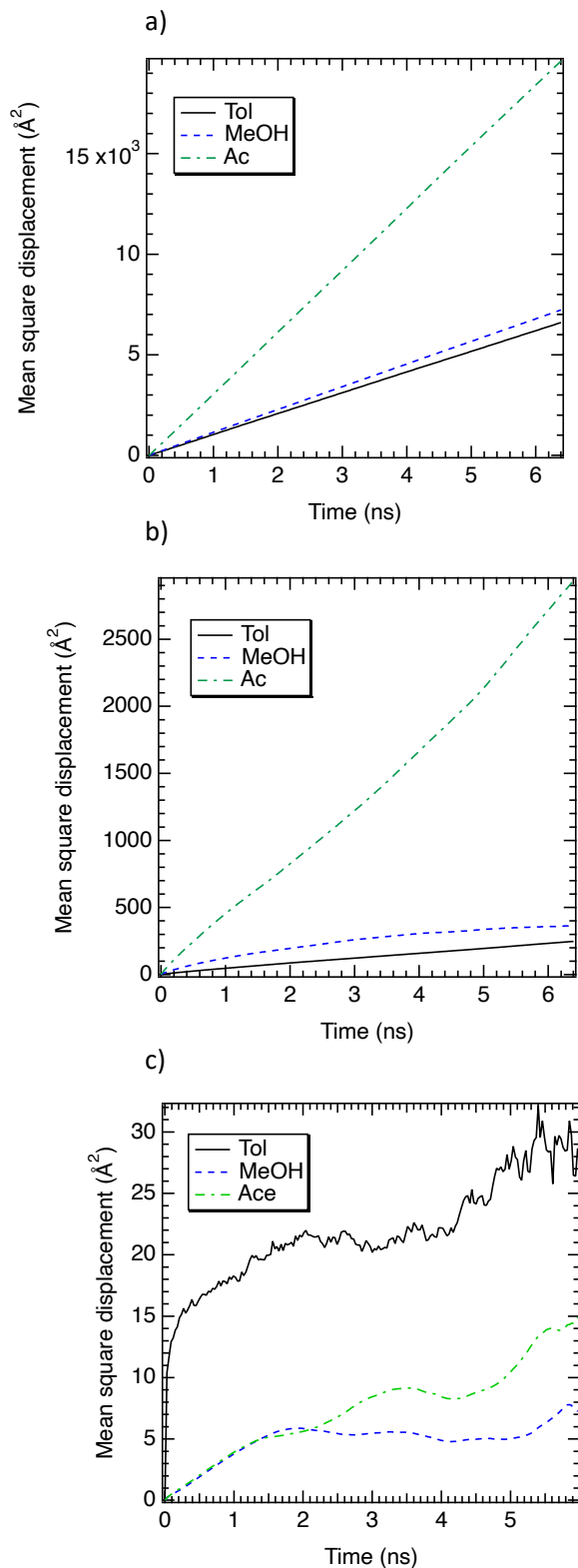


Figure 3: Mean square displacement of toluene (Tol), acetone (Ac), and methanol (MeOH) molecules as a function of time in a) the bulk phase a), b) in the PIM-1 membrane, and c) in the P84 membrane.

vents (Tol and Ac) that exhibit weaker affinity towards the P84 membrane (as discussed hereafter). The loss of hydrogen bonds between MeOH molecules confined in the PIM-1 membrane was much lower (only about 0.2 bond per molecule; see Figure 4b) due to the high swelling of PIM-1, which led to free volumes in the membrane that were wide enough to accommodate a large number of MeOH molecules that could interact with each other almost as in the bulk phase.

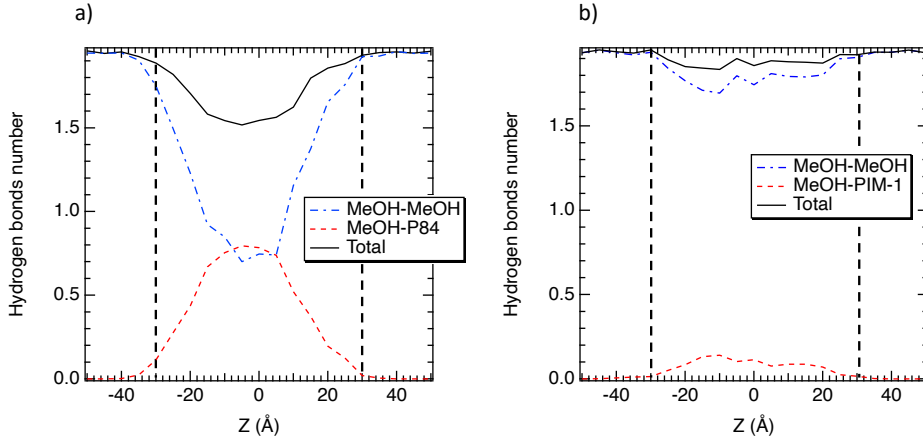


Figure 4: z-axis profile of the number of hydrogen bonds (per molecule) formed between MeOH molecules themselves and between MeOH molecules and the membrane in a) the P84 membrane and b) the PIM-1 membrane. The dashed vertical lines indicate the membrane/solvent interfaces.

The radial distribution functions (RDFs) between the center of mass of the MeOH molecules and the oxygen atoms, nitrogen atoms and aromatic rings of the PIM-1 membrane are reported in Figure 5a. The nitrogen atoms and the aromatic rings of the PIM-1 membrane appeared to be the preferential sites of interactions with the MeOH molecules, with a main peak of the RDF located below 2 \AA which indicates quite strong attractive interactions.¹³ The RDF between the oxygen atoms of the PIM-1 membrane and the MeOH molecules also exhibited a first peak located at the same distance but with a very small amplitude, thus indicating less pairwise interactions compared to the interactions between MeOH and the nitrogen atoms and aromatic rings of the membrane. Figures 5b and 5c show less favorable interactions between the PIM-1 membrane and the Ac and Tol molecules as the first peak of the corresponding RDFs was found above 4 \AA . Unlike the PIM-1 membrane, MeOH molecules were found to interact preferentially with the

oxygen atoms of the P84 membrane (see Figure 5d) while the main peaks of the RDF between MeOH and the membrane nitrogen atoms and aromatic rings were found around 4 Å and 5 Å, respectively. The different preferential sites of interactions between MeOH and the two membranes (the nitrogen atoms and the oxygen atoms for the PIM-1 and P84 membranes, respectively) can be explained by the difference in accessibility of the nitrogen and oxygen atoms in the two membranes (see chemical structures in Figures 1a and 1b). Figure 5e shows that the RDF between the Tol molecules and the nitrogen atoms of the P84 membrane exhibits a first peak located at 3.8 Å whereas the first peak of the Tol-O RDF is located farther (5 Å) and no peak is observed in the RDF between the Tol molecules and the aromatic rings of the P84 membrane. Thus, compared to the oxygen atoms and aromatic rings, the nitrogen atoms of the P84 membrane are preferential interaction sites for Tol molecules (although these interactions are much less favorable than those between MeOH molecules and the oxygen atoms of the P84 membrane). Similarly, Figure 5f shows that the nitrogen atoms of the P84 membrane are preferential interaction sites with the Ac molecules. Eventually, it can be concluded from Figures 5d, 5e and 5f that the P84 membrane / solvent affinity follows the order MeOH > Ac > Tol and is inversely correlated with the sequence of MSDs observed in 3c (Tol > Ac > MeOH).

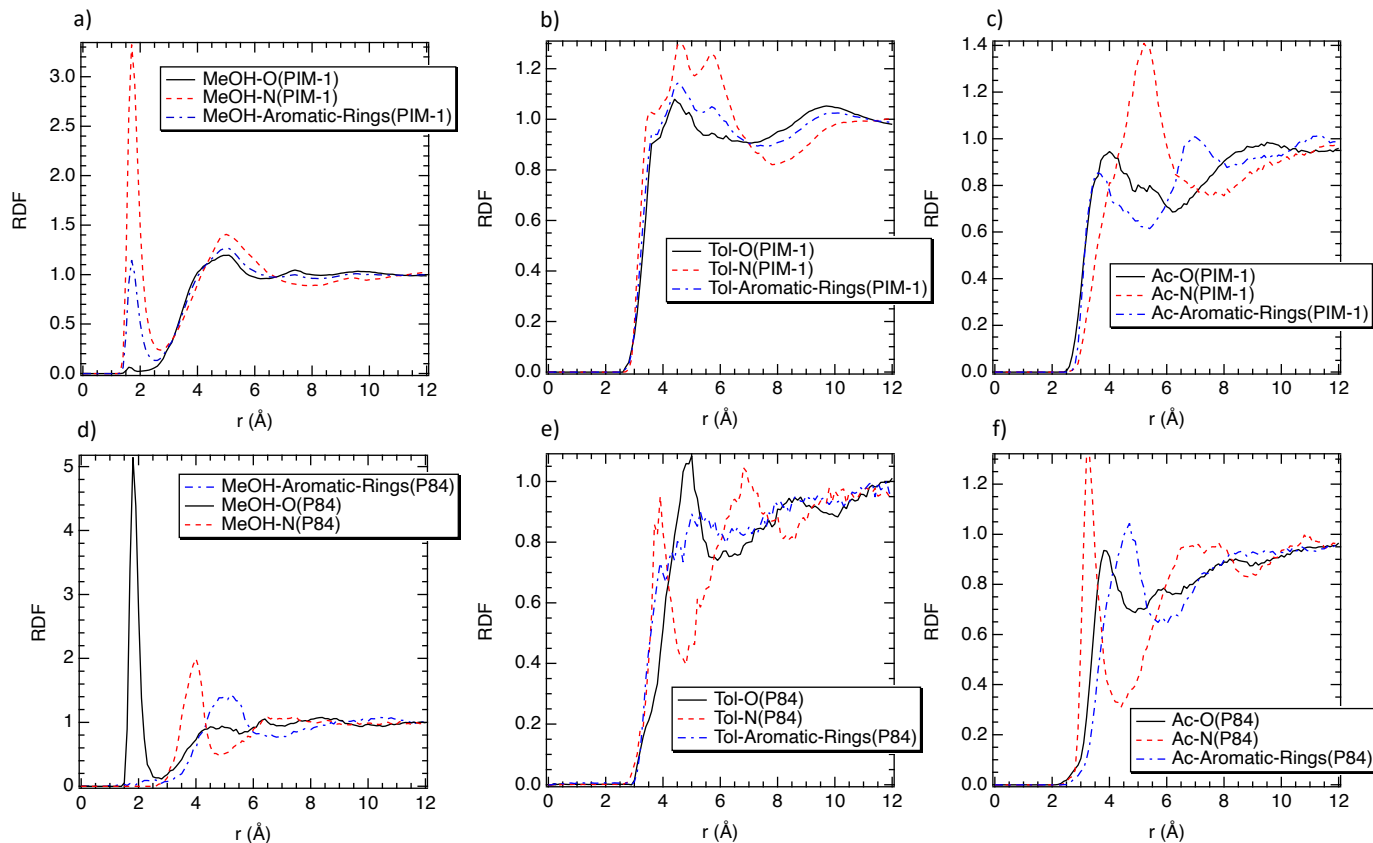


Figure 5: Radial distribution functions (RDF) between the center of mass of the solvent molecules and the oxygen atoms, nitrogen atoms and aromatic rings of the PIM-1 membrane (figures a, b and c) and the P84 membrane (figures d, e and f).

Conclusion

Molecular dynamic simulations of toluene, acetone and methanol within PIM-1 and P84 polyimide membranes were carried out. The uptake of the various organic solvents by the two polymer membranes was determined by explicit modeling of the polymer/solvent interfaces. The PIM-1 membrane was found to swell strongly in the three solvents unlike the P84 membrane. It results from the higher rigidity of the PIM-1 backbone that prevents the intricate entanglement of the polymer chains, thus favoring the formation of large free volumes and larger solvent uptake (up to 102 %wt for acetone). The translational dynamics of the solvent molecules in the PIM-1 membrane was found to be correlated with the solvent viscosity due to the relatively large pores of this membrane, which allowed the solvents to maintain a bulk-like behavior. Unlike the PIM-1 membrane, the solvent

uptake by the P84 polyimide membrane was found very low (less than 15 %wt) for the three solvents under consideration, which could be explained by the strong entanglement of the polymer chains due to the more flexible backbone of the P84 polyimide (compared to PIM-1). The three solvents were found to exhibit a much slower translational dynamics in the P84 membrane than in the PIM-1 membrane (with MSDs smaller by about two orders of magnitude). Moreover, unlike the PIM-1 membrane, no correlation was found between the MSDs of the solvents confined in the P84 membrane and their viscosities but the MSDs were found to decrease with increasing membrane / solvent specific interactions. The latter were investigated through the radial distribution functions between the center of mass of the solvents and some specific sites of the membranes. A strong affinity between methanol and the P84 membrane was highlighted through the formation of a substantial number of hydrogen bonds between the confined methanol molecules and the membrane, which contributed to partly compensate the loss of hydrogen bonds between methanol molecules as a result of the extreme confinement in the P84 membrane. It was also shown that the preferential sites of interactions with methanol are different in the PIM-1 membrane (nitrogen atoms) and in the P84 membrane (oxygen atoms) due to different accessibility of these atoms in the two membranes.

Competing financial interests

The authors declare no competing financial interests.

Acknowledgements

We are grateful to the "Agence Nationale de la Recherche" (ANR) for its financial support through the project "MANIAC" (ANR-18-CE07-0028-02).

References

1. Castel, C.; Favre, E. Membrane separations and energy efficiency. *J. Mem. Sci.* **2018**, *548*, 345–357.

2. R.P.Lively,; Sholl, D. From water to organics in membrane separations. *Nat. Mater.* **2017**, *16*, 276–279.
3. Marchetti, P.; Solomon, M. J.; Szekely, G.; Livingston, A. Molecular separation with organic solvent nanofiltration: a critical review. *Chem. Rev.* **2014**, *114*, 10735–107806.
4. Gould, R.; White, L.; Wildemuth, C. Membrane separation in solvent lube dewaxing. *Environ. Prog.* **2001**, *20*, 12–16.
5. Darvishmanesh, S.; Firoozpour, L.; vanneste, J.; Luis, P.; Degrève, J.; der Bruggen, B. V. Performance of solvent resistant nanofiltration membranes for purification of residual solvent in the pharmaceutical industry: experiments and simulation. *Green Chem.* **2011**, *13*, 3476–3483.
6. Keraani, A.; Renouard, T.; Fishmeister, C.; Bruneau, C.; Rabiller-Baudry, M. Recovery of Enlarged Olefin Metathesis Catalysts by Nanofiltration in an Eco-Friendly Solvent. *ChemSusChem* **2008**, *1*, 927.
7. Favas, E.; Kouvelos, E.; Romanos, G.; Pilatos, G.; Mitropoulos, A.; Kanellopulos, N. Characterization of highly selective microporous carbon hollow fiber membranes prepared from a commercial co-polyimide precursor. *J. Porous Mater* **2008**, *15*, 625–633.
8. Fritsch, D.; Merten, P.; Heinrich, K.; ans M. Priske, M. L. High performance organic solvent nanofiltration membranes: Development and thorough testing of thin film composite membranes made of polymers of intrinsic microporosity (PIMs). *J. Mem. Sci.* **2012**, *401-402*, 222–231.
9. Xu, Q.; Jiang, J. Computational characterisation of ultrathin polymer membranes in liquids. *Macromolecules* **2018**, *51*, 7169–7177.
10. Liu, J.; Xu, Q.; Jiang, J. A molecular simulation protocol for swelling and organic solvent nanofiltration of polymer membranes. *J. Mem. Sci.* **2019**, *573*, 639–646.

11. Xu, Q.; Jiang, J. Molecular simulations of liquid separations in polymer membranes. *Current Opinion in Chem. Eng.* **2020**, *28*, 66–74.
12. Xu, Q.; Jiang, J. Effects of functionalization on the nanofiltration performance of PIM-1: Molecular simulation investigation. *J. Mem. Sci.* **2019**, *591*, 117357.
13. Ouinten, M.; Szymczyk, A.; Ghoufi, A. Interactions between methanol/toluene binary mixtures and an organic solvent nanofiltration PIM-1 membrane. *J. Mol. Liq.* **2022**, *357*, 119146.
14. Xin, Y.; Yin, F. Influence of water on the recovery of lube oil dewaxing solvent using P84 polyimide membrane: A combination of experiment and molecular simulation. *Chemistry select* **2020**, *5*, 2094–2102.
15. Abbott, L.; Hughes, J.; Colina, C. Virtual Synthesis of Thermally Cross-Linked Copolymers from a Novel implementation of Polymatic. *J. Phys. Chem. B* **2014**, *118*, 1916–1924.
16. Plimton, S. Fast parallel algorithms for short range molecular dynamics. *J. Comp. Phys.* **1995**, *117*, 1–19.
17. Larsen, G.; Lin, P.; Hart, K.; Colina, C. Molecular Simulations of PIM-1-like Polymers of Intrinsic Microporosity. *Macromolecules* **2011**, *44*, 6944–5951.
18. Budd, P.; Elabas, E.; Ghanem, B.; Makhseed, S.; McKeown, N.; Msayib, K.; Tattershall, C.; Wang, D. Solution-Processed Organophilic Membrane Derived from a Polymer of Intrinsic Microporosity. *Adv. Mater.* **2004**, *16*, 456–459.
19. Hofmann, D.; Fritz, L.; Ulbrich, J.; Schepers, C.; Bohning, M. Detailed-Atomistic Molecular Modeling of Small Molecule Diffusion and Solution Processes in Polymeric Membrane Materials. *Macromol. Theory Simul.* **2000**, *9*, 293.
20. Semino, R.; Ramsahye, N.; Ghoufi, A.; Maurin, G. Microscopic model of the metal-organic framework/Polymer interface: A first step toward understanding the com-

- patibility in Mixed Matrix Membranes. *ACS Appl. Mater. & Interfaces* **2016**, *8*, 809–819.
21. Gilois, B.; Goujon, F.; Fleury, A.; Soldera, A.; Ghoufi, A. Water nano-diffusion through the Nafion fuel cell membrane. *J. Memb. Sci.* **2020**, *602*, 117958.
 22. Wang, J.; Wolf, R.; Caldwell, J.; Kollman, P.; Case, D. Development and Testing of a General Amber Force Field. *J. Comp. Chem.* **2004**, *25*, 1157–1174.
 23. Frentrup, H.; Hart, K.; Colina, C.; Muller, E. In Silico determination of gas permeabilities by non-equilibrium molecular dynamics: CO₂ and He through PIM-1. *Membranes* **2015**, *5*, 99–119.
 24. Jorgensen, W.; Maxwell, D.; Tirado-Rives, J. Development and Testing of the OPLS All-Atom Force Field on Conformational Energetics and Properties of Organic Liquids. *J. Am. Chem. Soc.* **1996**, *118*, 11225.
 25. Essafri, I.; Ghoufi, A. Microstructure of nonideal methanol binary liquid mixtures. *Phys. Rev. E* **2019**, *99*, 062607.
 26. Ewald, P. Die Berechnung optischer und elektrostatischer Gitterpotentiale. *Ann. Phys.* **1921**, *64*, 253.
 27. Darden, T.; Perera, L.; Pedersen, L. New tricks for modelers from the crystallography toolkit: the particle mesh Ewald algorithm and its use in nucleic acid simulations. *Structure* **1999**, *7*, R55.
 28. Hoover, W. Canonical dynamics: Equilibrium phase-space distributions. *Phys. Rev. A* **1985**, *31*, 1695.
 29. Ghoufi, A.; Morineau, D.; Lefort, R.; Hureau, I.; Hennous, L.; Zhu, H.; Szymczyk, A.; Malfreyt, P.; Maurin, G. Molecular simulations of confined liquids: An alternative to the grand canonical Monte Carlo simulations. *J. Chem. Phys.* **2011**, *134*, 074104.

30. Willems, T.; Rycroft, C.; Kazi, M.; Meza, J.; Haranczyk, M. Algorithms and tools for high-throughput geometry- based analysis of crystalline porous materials. *Micr. Meso. Mater.* **2012**, *149*, 134–141.
31. Luzar, A.; Chandler, D. Effect of Environnement on Hydrogen Bond Dynamics in Liquid Water. *Phys. Rev. letters* **1996**, *76*, 928.